ADVANCED MATERIALS INTERFACES

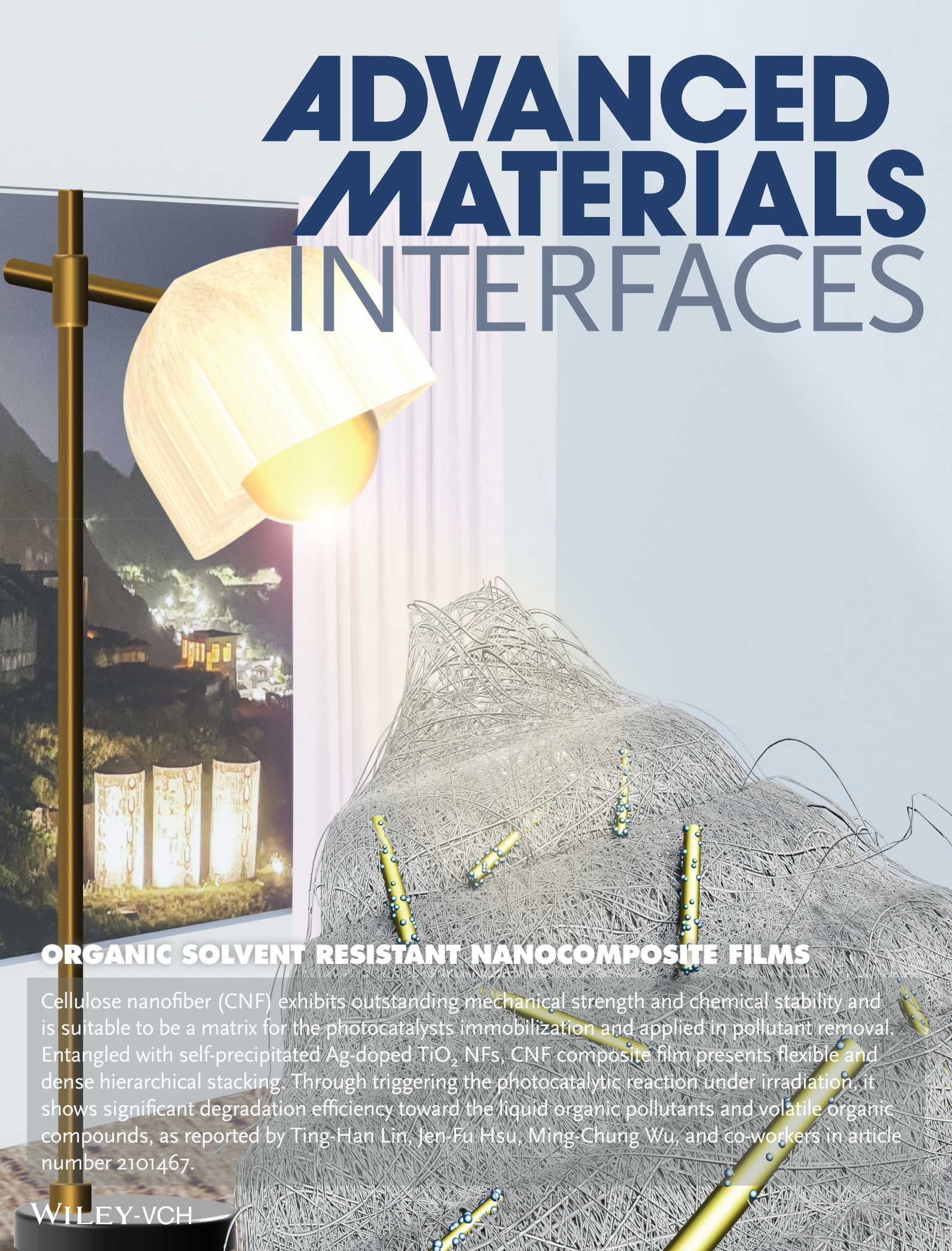

ORGANIC SOLVENT RESISTANT NANOCOMPOSITE FILMS

Cellulose nanofiber (CNF) exhibits outstanding mechanical strength and chemical stability and is suitable to be a matrix for the photocatalysts immobilization and applied in pollutant removal. Entangled with self-precipitated Ag-doped TiO_2 NFs, CNF composite film presents flexible and dense hierarchical stacking. Through triggering the photocatalytic reaction under irradiation, it shows significant degradation efficiency toward the liquid organic pollutants and volatile organic compounds, as reported by Ting-Han Lin, Jen-Fu Hsu, Ming-Chung Wu, and co-workers in article number 2101467.

WILEY-VCH

ADVANCED MATERIALS INTERFACES
www.advmatinterfaces.de

Organic Solvent Resistant Nanocomposite Films Made from Self-precipitated Ag/TiO_2 Nanofibers and Cellulose Nanofiber for Harmful Volatile Organic Compounds Photodegradation

Ting-Han Lin, Yu-Han Liao, Kun-Mu Lee, Yin-Hsuan Chang, Kai-Hsiang Hsu, Jen-Fu Hsu, and Ming-Chung Wu**

Cellulose exhibits outstanding chemical stability, nontoxicity, and renewable ability and is regarded as a candidate for next-generation sustainable materials. After the nanofibrillation of cellulose, cellulose nanofiber (CNF) exhibits unique optical properties, good mechanical strength, and a high aspect ratio. It is suitable to be a matrix for the photocatalysts immobilization and applied in pollutant removal owing to its solvent resistance. Combined with 1D TiO_2, the network structure may be expected and beneficial for the charge transport of TiO_2 nanofibers. In this study, the flexible CNF composites film incorporated with various sizes and morphology of TiO_2 photocatalysts is fabricated. The relationship between the chemical and physical properties of the composite film and morphological features are discussed. The GIWAXS analysis shows that the entanglement of self-precipitated Ag-doped TiO_2 NFs (STNFs) and CNF induce the densely hierarchical stack and regular stacking orientation. For 30 day solvent resistance tests, various CNF composite films show outstanding stability in the acetone and dimethylformamide (DMF). In the photodegradation of methyl orange in ethanol, STNF/CNF film presents a high degradation efficiency of 87% and shows excellent stability of morphology and activity after three cycles. For volatile organic compound degradation, the degradation efficiencies toward methanol and DMF vapor are higher than 90%.

1. Introduction

The increasing awareness of sustainable development has led to an emphasis on organic pollutant removal. The elimination of the pollutant in wastewater or air can be realized by electrochemical, membrane technology, and photocatalysis.[1–8] Photocatalysis, a process using abundant and eco-friendly solar energy to trigger degradation, is thought of as a strong asset to environmental sustainability. The highly reactive oxidizing species generated from photocatalysts are indispensable for the oxidation of pollutants. The current efforts are focused on the aggregation of powder photocatalyst, catalytic cycles, carrier separation, and utilization of solar light.[9,10] Introducing photocatalytic materials in the membrane matrix gathers the requirement mentioned above and demonstrates the potential in the reusable photocatalyst and the pollution treatments.[11–13]

TiO_2 is an extensively used photocatalyst due to its thermal and chemical stability, environmental friendliness, and easy preparation.[14–16] The photocatalytic performance is highly dependent on its microstructure. Zero-dimensional TiO_2 nanoparticle holds a large surface area and broadened bandgap, and thus it could provide more active sites to enhance photocatalytic activity than that of high-dimensional materials. Developing TiO_2 nanoparticles is popular in the initial stage of the study. However, the drawbacks gradually emerged, such as its slow charge carrier transport caused by its inner defect and its limited light absorption due to its wide bandgap. Oppositely,

T.-H. Lin, Y.-H. Liao, K.-M. Lee, Y.-H. Chang, M.-C. Wu
Department of Chemical and Materials Engineering
Chang Gung University
Taoyuan 33302, Taiwan
E-mail: mingchungwu@cgu.edu.tw
K.-M. Lee, M.-C. Wu
Green Technology Research Center
Chang Gung University
Taoyuan 33302, Taiwan

The ORCID identification number(s) for the author(s) of this article can be found under https://doi.org/10.1002/admi.202101467.

DOI: 10.1002/admi.202101467

K.-M. Lee, K.-H. Hsu, J.-F. Hsu, M.-C. Wu
Division of Neonatology
Department of Pediatrics
Chang Gung Memorial Hospital
Linkou, Taoyuan 33305, Taiwan
E-mail: hsujanfu@cgmh.org.tw
J.-F. Hsu
School of Medicine
College of Medicine
Chang Gung University
Taoyuan 33302, Taiwan

the development of 1D (nanotubes, nanowires, and nanorods, etc.) TiO_2 nanomaterials attracted plenty of interest for their photocatalytic activity, efficient charge transport path, large specific surface area, and enhanced adsorption capacity.[17,18] In this framework, doping engineering is a rational method to overcome the limitation of its wide bandgap (3.2 eV).and broadens applications of TiO_2. Based on our previous studies, Ag-doped TiO_2 stands out from 11 kinds of transient metal-doped TiO_2 (Ag, Au, Co, Cr, Cu, Fe, Ni, Pd, Pt, Y, and Zn).[19,20] Ag-doped TiO_2 increased absorption in the visible range. Also, the surface plasmon resonance induced by Ag_2O facilitated the photodegradation performance and disinfection behavior.[21]

Cellulose is the most abundant natural and biodegradable polymer on earth. As a natural material, it can be extracted from wood, crop, and cotton.[22,23] Its intrinsic properties, including biocompatibility, biodegradation, chemical stability, nontoxicity, and renewable ability, make it be regarded as a potential sustainable material in the next generation.[24–28] Cellulose nanofiber (CNF) extracted from cellulose fibers has been reported to exhibit the superfine network structure, unique optical properties, good mechanical strength, and high aspect ratio.[29–33] Thus, CNF is considered as an ideal matrix material for the immobilization of photocatalysts. TEMPO-oxidation is an effective route to disintegrate the CNF in cellulose microfibril bundles due to its high yield of nanofabrillation, cost-effectiveness, and low energy consumption.[34,35] It contributes to the formation of the regioselective repulsive force between each nanofibril by modification of C6 carboxylate. The carboxylate groups on the C6 glucose unit provide new chemical functionality for further surface modification by chemical/physical grafting. The ligand substitution makes the CNF much compatible with other materials to extend its application.

For practical application of organic removal, immobilization of photocatalysts realizes the concepts of recycling and reusing. Many studies have revealed that TiO_2 and cellulose fibers show good compatibility for TiO_2 immobilization, and it can be attributed to the physical embedding by cellulose fibers.[12,13,36–38] The overall performances of the TiO_2/Cellulose composites are highly dependent on the dispersion of the TiO_2 in the cellulose matrix and exposure to the surrounding reactants. Improving the hydrophilicity of TiO_2 makes it well-dispersed and evenly embed cellulose fibers in the aqueous precursor, further getting a smooth composite film appearance. Wang et al. proposed a surface modification of TiO_2 by UV light illumination. The irradiation forms a temporary oxygen vacancy on the surface of TiO_2. The oxygen vacancy at the two coordinated oxygen bridging sites is further occupied by H_2O or OH^- and thus enriches its hydrophilic property.[39] Moreover, the morphology of the second phase usually dominates mechanical properties. It is rationally predicted that nanofiber-shaped materials can probably be combined with CNF to form the dense, flexible, and freestanding composite film because of the accordance size between each other. There are lots of studies mainly devoted to CNF composite film. But seldom of them discuss the relationship between the morphological effects and photocatalytic performance.

This work proposes a method to prepare the multifunctional TiO_2/CNF composite film with excellent flexibility, solvent resistance, and high photocatalytic activity for organic pollution removal. CNF is disintegrated from pulp and modified by using the TEMPO-mediated oxidation method. A series of TiO_2 photocatalysts with different morphology and size are incorporated with CNF to construct freestanding films. To clarify the superior incorporation of TiO_2 nanofiber in the composite film, we study the hierarchical structure features examined by the grazing-incidence wide-angle x-ray scattering (GIWAXS) patterns. Also, the cross-sectional elemental mapping perfectly reveals the construction of the composite framework, which is crucial evidence for their physicochemical properties. For the application, the excellent organic solvent resistances toward the acetone and dimethylformamide are demonstrated. In addition, the photodegradation of pollutants involving organic dye solution and volatile organic compound (VOC) vapors were performed.

2. Results and Discussion

2.1. Hierarchical Structure Investigation

Cellulose nanofiber is disintegrated from the pulp by TEMPO oxidation, followed by mechanical agitation. TEMPO-oxidized CNF and related CNF film were observed by atomic force microscopy, as shown in Figure S1 (Supporting Information). CNF featured a uniform size and entangled with adjacent fibers. The average diameter and length are 18.1 ± 4.1 and 1168.3 ± 281.1 nm, respectively (Figure S2, Supporting Information) It is noted that the cellulose nanofibrillation was successful through the TEMPO-mediated oxidation, followed by $NaBH_4$ postreduction. After solution casting and drying, the induced hydrogen bonding which interacts between nanofibers makes CNF be assembled orderly and densely. To extend the CNF films application, we fabricated a photocatalyst/CNF composite film for the photodegradation of organic pollution. The various sorts of photocatalysts were incorporated with CNF hydrogel, constructing freestanding films. To investigate the size and morphological effect on CNF composite material, we demonstrated the morphologies of various TiO_2 photocatalysts, including TMP (TiO_2 microsized particles, $D_{avg} \approx 200$ nm) and TNP (TiO_2 nanoparticles, $D_{avg} \approx 20$ nm), TNF (TiO_2 nanofibers, $D_{avg} \approx 50$ nm), and STNF (self-precipitated silver-doped TiO_2 nanofibers, $D_{avg} \approx 50$ nm) (**Figure 1**). Generally, both TMP and TNP were the typical photocatalysts for organic removal. The latter was as-synthesized photocatalysts with nanofibrous morphologies that held a high crystalline and efficient performance on photocatalytic reactions. Especially, STNF had the heterostructure constructed by 1D TiO_2 nanofiber and 0D silver nanoparticles, reported in Figure S3 (Supporting Information).[21,40]

The hierarchical structure of CNF composite films was a crucial factor, determining their physiochemical properties. TiO_2 incorporation of different sizes and morphologies might induce unexpected effects on the composite properties and application performance. Herein, we reported the cross-sectional images of composite films by field-emission scanning electron microscopy (FESEM), as shown in **Figure 2** and Figure S4 (Supporting Information). The regular arrangement of fibers was observed in the CNF film and fibers stacked on the vertical orientation (Figure S4, Supporting Information). As the TiO_2 particles

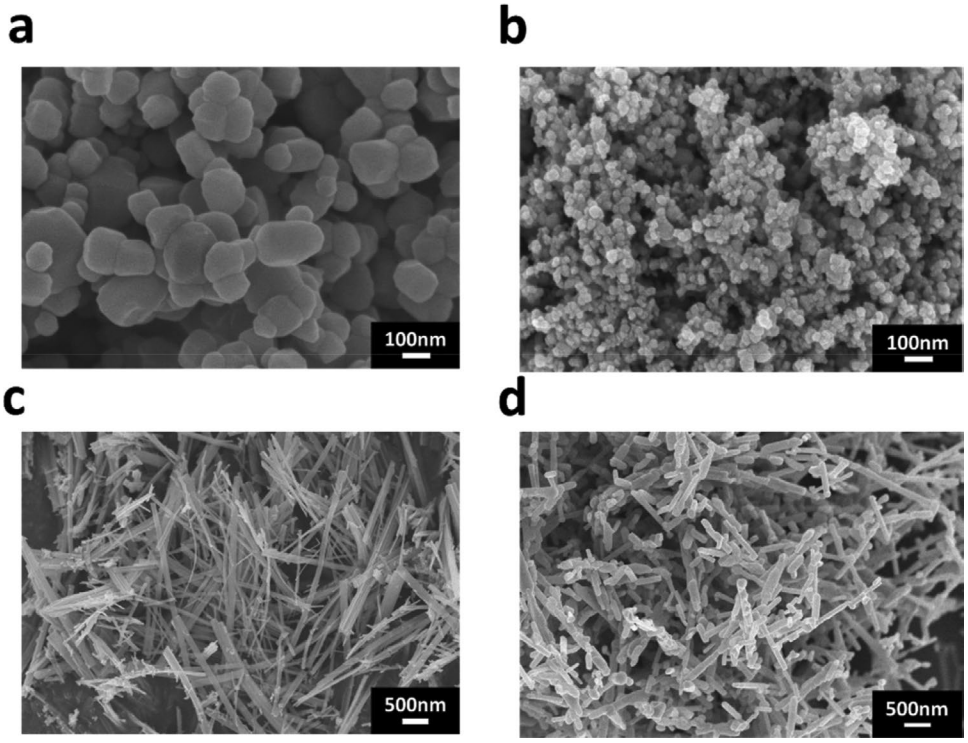

Figure 1. FESEM images of a) TMP, b) TNP, c) TNF, and d) STNF.

embedded in the CNF hierarchical structure, the heterogeneous incorporation thoroughly changed the aligned arrangement (Figure 2a-1 and Figure 2b-1). Particularly, in the inset of magnified images, a clear aggregation of both TMP (Figure 2a-1) and TNP (Figure 2b-1) was observed, thus compressing nearby CNF and causing CNF stacking distortion. On the contrary, neither TNF (Figure 2c-1) nor STNF (Figure 2c-1) incorporation were entangled and embedded with the CNF and maintained the original vertical orientation. It concluded that the different filler morphologies gradually influence the matrix arrangement, and

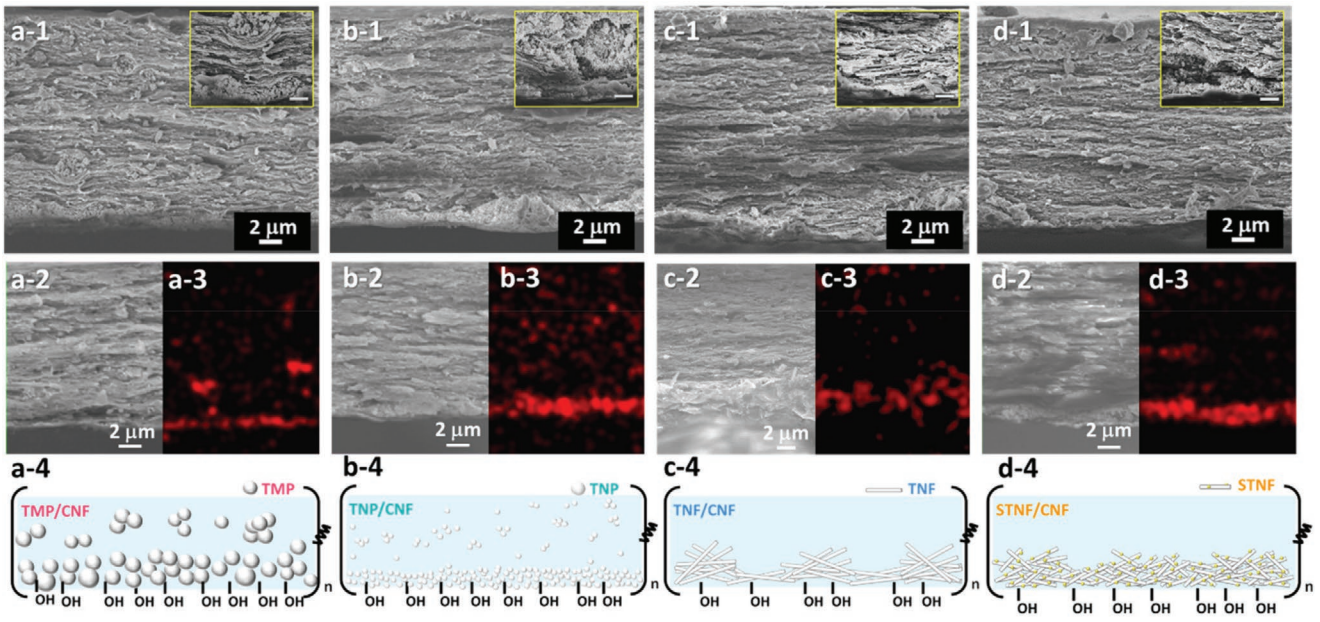

Figure 2. Observation of the effect of different fillers on CNF composite stacking: a–d-1) Cross-sectional FESEM images, and magnified images of photocatalyst (inset), a–d-2) magnified images of film boundary and a–d-3) EDS mapping of Ti distribution, and a–d-4) schematics of TiO_2 distribution in the film; a) TMP, b) TNP, c) TNF, and d) STNF.

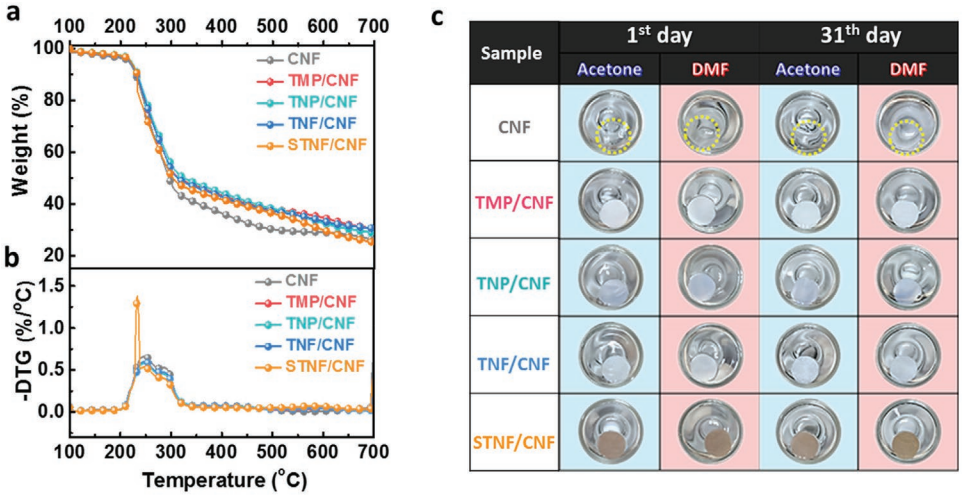

Figure 3. Thermal and chemical resistance test for CNF composite: a) Thermogravimetric curves and b) derivative thermogravimetric curves of various TiO_2/CNF composite films, and c) Illustration of solvent resistance by using various TiO_2/CNF against acetone and DMF.

similar dimensional materials help the composite maintain the intrinsic CNF stacking structure. To unveil the hierarchical construction, we performed the cross-sectional elemental mapping to depict the distribution of incorporated TiO_2 materials in the composite films, as shown in Figures 2 and 3. From the mapping results, both TMP and TNP are deposited at the bottom and randomly embedded in the CNF hierarchical structure. It could result in the low crystallinity of CNF film due to the disordered arrangement of CNF and the elimination of strong hydrogen bonding forming between the CNF. On the contrary, both TNF and STNF mainly stacked at the bottom of composite film and rarely appeared between the orientated CNF. The partial TiO_2 NFs even entangled with the bottom CNF (Figure 2c,d). In addition, we observed both sides of the CNF and CNF composite films. It is indicated that the surface morphologies were highly related to the corresponding cross-sectional images (Figure S5, Supporting Information). Herein, we illustrated the scheme for various composite films (Figure 2a–d-4). It can be expected to the dense stacking of CNF, leading to high crystallinity of CNF composite film and better mechanical properties.

2.2. Physicochemical Properties

The diversity of the hierarchical structure of CNF composite film dominates the physicochemical properties. First, we evaluated the thermal stability of composite films by thermogravimetric analysis as demonstrated in (**Figure 3**a). The derivative thermograms (DTG) were further plotted for a better understanding of the results and were shown in (Figure 3b). From the results of the derivative thermogram analysis, two broad peaks located at around 248 and 290 °C indicated an obvious degradation of CNF and TiO_2/CNF composite. Both degradation temperatures are specified to primary degradation of the cellulose matrix, a carboxylate group, and a fundamental glucose unit during the heating scans. Significantly, the STNF/CNF composite film showed a specific peak in the DTG curve because of the silver nanoparticles that reacted with a carboxylate group of cellulose chains. It can be found that all the CNF and TiO_2/CNF composite films are thermally cracked at a temperature that higher than 200 °C. Compared to the CNF film, the thermal decomposition temperatures (T_d) of various composite films were raised by adding TiO_2, and the T_d of each material is summarized in **Table 1**. TiO_2/CNF showed a delayed cracking behavior, which indicates that TiO_2 can improve thermal stability. The solvent resistance of various TiO_2/CNF composite films was demonstrated for practical application, as shown in Figure 3c and Figure S6 (Supporting Information). After the samples were immersed in pure acetone and dimethylformamide (DMF) for 31 days, all composite films still maintained their original appearances. The results depict that all composites exhibit excellent resistance to acetone and DMF. It was ascribed to the high chemical stability of cellulose.

The optical properties of various TiO_2/CNF composite films are shown in **Figure 4**a. CNF film showed low absorbance and appeared highly transparent. Mechanical fibrillation treatment can significantly improve the entanglement between the fibers. The bundled fiber was separated and smaller nanofibers were obtained, effectively reducing the optical behavior such as refraction and diffraction of light in the film. Therefore, the CNF film exhibits a highly transparent characteristic. Due to the low absorbance of cellulose nanofibers, all of the composite films show the intrinsic absorption of TiO_2. Besides, TiO_2, not being well embedded in CNF, also caused the light to scatter and to interfere with the inherent absorption of the visible light

Table 1. Physical properties, including thermal decomposition point and crystallinity index.

Specimen	T_d [°C]	Crystallinity index [%]
CNF	216	64.4
TMP/CNF	219	67.1
TNP/CNF	221	67.3
TNF/CNF	218	67.8
STNF/CNF	220	69.0

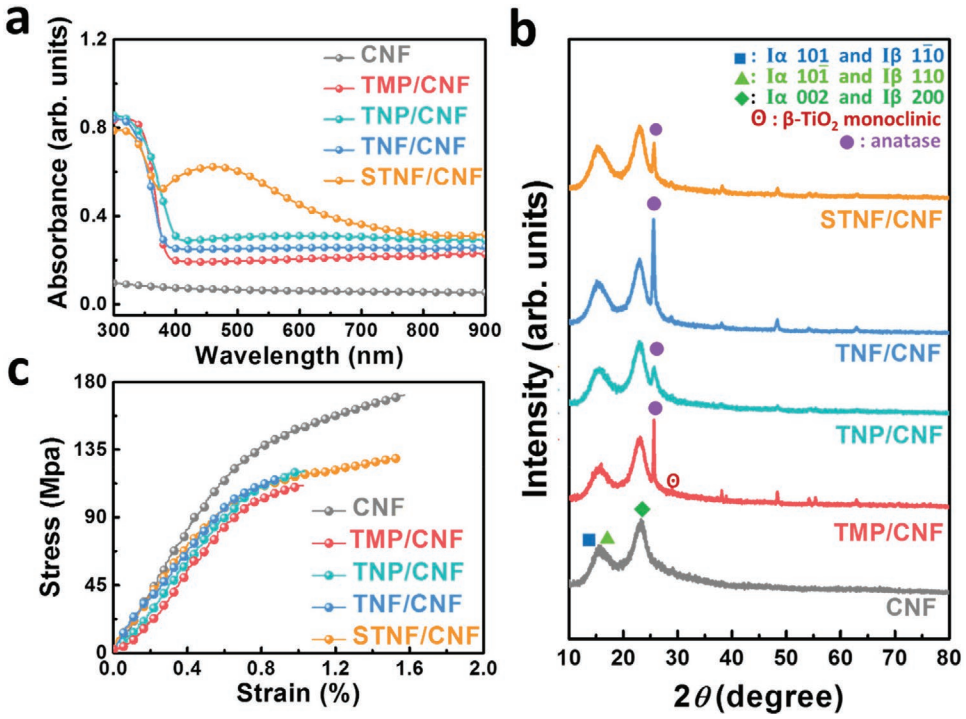

Figure 4. Characterization of optical property, crystallinity, and tensile strength for all composite: a) absorption spectra, b) XRD patterns, and c) stress–strain curves of CNF film and various TiO_2/CNF composite films incorporated with TMP, TNP, TNF, and STNF.

region. All the TiO_2 showed enhanced absorption in the visible light region, but the STNF further showed a strong SPR band. Coupling with incident light at a specific wavelength, this drove the free electrons on the Ag into oscillation, which may achieve photocatalytic superiority. The crystal structures of various TiO_2/CNF composite films are presented in Figure 4b. The diffraction peaks of cellulose at 2θ of 15.5°, 15.9°, and 22.2° were indexed as Iα (triclinic) and Iβ (monoclinic) phases due to the allomorph of cellulose. The typical diffraction peak of anatase TiO_2 phase, (101) plane, was also observed at 2θ of 25.3°. The detailed crystal structure of various TiO_2 photocatalysts was reported in supporting information (Figure S7, Supporting Information). Anatase phase TiO_2, rutile phase TiO_2, and silver oxide were indexed completely. It indicated that TMP was constructed pristine anatase TiO_2, and TNP contained a mixture phase of anatase and rutile. Remarkably, as-prepared TNF and STNF showed strong diffraction peaks of anatase phase, denoted that high crystalline was expected as same as our previous study.[21] Also, a weak diffraction peak of silver derivates can be observed at 2θ of 32.3°. It is depicted that silver nanoparticles were located on TiO_2 nanofibers, being consistent with HRTEM observation (Figure S3, Supporting Information). On top of the XRD pattern, we further investigated crystallinity, which is a crucial issue for the mechanical properties. The crystallinity of cellulose can be quantified by using the equation of crystallinity index, which is described as follows

$$\text{Crystallinity index} = \left[(I_{200} - I_{\text{am}})/I_{200}\right] \times 100\% \quad (1)$$

where I_{200} represents the X-ray diffraction intensity of (200) plane at 2θ of ≈22.5°, and I_{am} represents the intensity of the amorphous region at 2θ of ≈18°. Cellulose is an allomorph of two crystalline forms, including triclinic α phase and monoclinic β phase. From Table 1, the crystallinity index of composite films was improved, indicating that the incorporation of heterogeneous materials led to the compression of cellulose nanofiber to stack much densely. Moreover, with the TiO_2 nanofibers like TNF and STNF, their crystallinity indices are higher than those of TMP and TNP. It showed that similar fiber morphology not only maintained the crystalline structure but also improved fiber stacking. To discover the relationship between the mechanical properties and hierarchical structure, we further quantified mechanical indices of various composite films. Based on the standard practice of ASTM D638-10 for the fabrication of testing samples, the stress–strain curve and related results were shown in Figure 4c and **Table 2**. Table 2 summarizes the mechanical properties of various TiO_2/CNF films. It can be observed that the average tensile strength of CNF incorporated with TNF is higher than that of TiO_2 particles. It was attributed to the relatively low disordered arrangement in the TNF/CNF film and was consistent with the SEM results.

2.3. GIWAXS Analysis

Herein, we revealed the arrangement transformation of CNF in the hierarchical structure by probing the grazing incident wide angle X-ray scattering (GIWAXS) measurement using the synchrotron radiation (λ = 1.021 Å). The regular arrangement of CNF can be observed in **Figure 5**a, showing the robust diffraction intensity in the 2D pattern. It performed the typical diffraction at around q = 10.5 and 15.5 nm^{-1} (Figure 5f). The significant

Table 2. Mechanical properties of various TiO_2/CNF composite films.

Sample name	Average tensile strength [MPa]	Maximum tensile strength [MPa]	Elongation at break [%]	Young's modulus [GPa]
CNF	156.5 ± 19.1	171.5	1.37 ± 0.54	22.36 ± 2.97
TMP/CNF	104.2 ± 7.5	112.4	1.72 ± 0.41	9.86 ± 2.26
TNP/CNF	117.7 ± 8.5	135.5	1.12 ± 0.37	16.01 ± 1.65
TNF/CNF	119.8 ± 9.8	134.1	1.10 ± 0.28	16.16 ± 1.66
STNF/CNF	122.5 ± 9.2	136.2	1.34 ± 0.48	16.21 ± 1.44

diffraction at $q = 15.5$ nm^{-1} was referred to Iα (100) and Iβ (200) plane. That can rationally speculate about inducing the vertical stack of CNF. From the Azimuth angle plots ((Figure 5g), it implied that most of the nanofibers stacked along in the out-of-plane direction, and some nanofibers entangled randomly like a distorted bundle. It also suggested a strong interaction of hydrogen bonding between each fiber and led to a compacted packing. When CNF was incorporated with TiO_2 particles, the diffraction intensity of TiO_2/CNF film in the 1D integration diagram decreased (Figure 5f). Compared to the incorporation of TMP (Figure 5b), CNF incorporated with TNP (Figure 5c) showed a lower diffraction intensity due to the nanoparticles embedded randomly in the CNF hierarchical structure. Such nano-scaled particles could be well-embedded thoroughly with

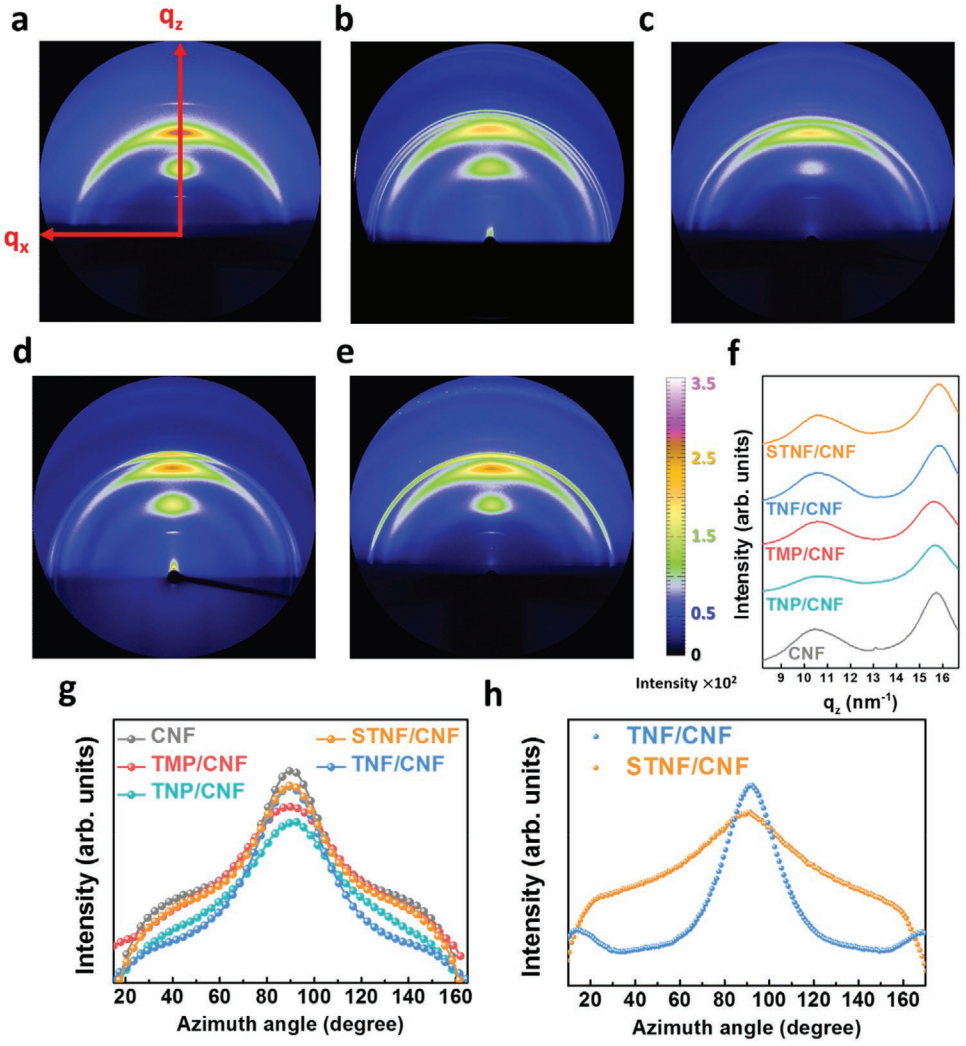

Figure 5. 2D GIWAXS patterns of a) CNF and various CNF composite films incorporated with b) TMP, c) TNP, d) TNF and e) STNF, f) 1D patterns of out-of-plane line cut, and Azimuth intensity plots corresponding to a–e) along the ring at g) 15.5 nm^{-1} for CNF crystal and h) 17.5 nm^{-1} for anatase phase of TiO_2.

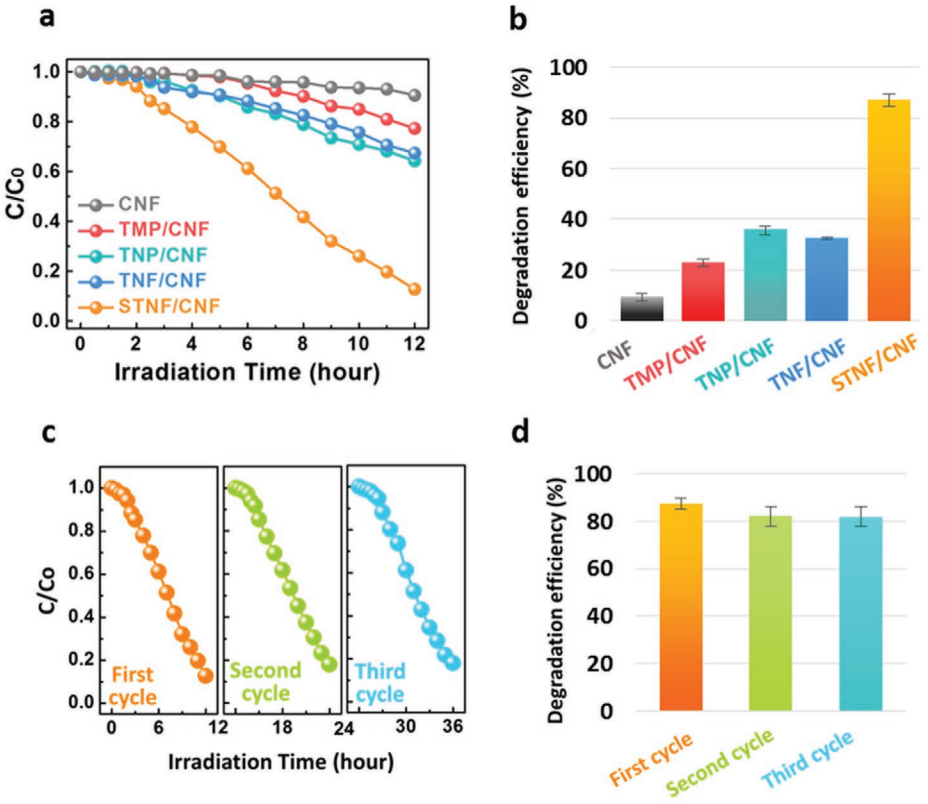

Figure 6. Photocatalytic activity test of CNF and CNF composites: a) photodegradation curves and b) the related bar graph plots of degradation efficiency of CNF and various CNF composite films; c) the recyclability test of STNF/CNF film and d) the related bar graph plots of degradation efficiency toward methyl orange in ethanol.

CNF, further disordering the CNF vertical packing and bundles entanglement. Thus, in Figure 5g, the overall diffraction intensity at q = 15.5 nm^{-1} was lower than it of pristine CNF at all Azimuth angles. The reason that TMP/CNF maintained better diffraction intensity was also attributed to most microsized particles aggregated, not thoroughly inserted into every CNF. However, it could lead to the noncontinuous CNF arrangement in the horizontal orientation due to the broken linkage of CNF. It was proved that the average tensile strength was the lowest. Furthermore, we noticed that the GIWAXS pattern of TNF/CNF (Figure 5d,f) and STNF/CNF (Figure 5e,f) presented higher intensity than that of TiO_2 particles (TMP and TNP) at q = 15.5 nm^{-1}. Considering the previous cross-section SEM observation, we realized that, in both films, TiO_2 stacked at the bottom of the composite film, and a few entanglements were perceived. It prevented the intense disordering of CNF, but TiO_2 NFs might anchor into the CNF at the interface. In the Azimuth angle plot (Figure 5g), the intensities were close to pristine CNF. Notably, CNF incorporated with pristine TiO_2 NFs showed similar intensity at the angle of 90° but showed a lower intensity at angles ranging from 20° to 60° and 120° to 160°. It implied that CNF preferred to orient along in out-of-plane direction compared to that of STNF (Figure 5h). On the contrary, STNF/CNF presented wide intensity similar to CNF film. Further integrating the Azimuth angle at q = 15.5 nm^{-1} for the interpretation of TNF arrangement, we found that the TNF also preferred to stack in the vertical orientation, whereas STNF stacked randomly. It was speculated that STNF exhibited dispersion in the CNF aqueous due to the pretreatment of UV irradiation. Based on the established mechanism of photocatalyst, when the STNF were irradiated by UV light, electron-hole pairs separated due to the heterojunction of silver NPs. The photoinduced electrons passed through the Schottky barrier, and the holes remain on the surface of TiO_2 NFs.[21] The hole-rich surface of TiO_2 possibly attracts to the negative carboxylate group of TEMPO-oxidized CNF, further compacting entanglement. After the drying process, its preferred orientation would be dominated by the CNF arrangement, and which is highly related to the CNF matrix. Therefore, the crystalline of CNF can be maintained and allowing the average tensile strength of STNF/CNF being the highest among various composite films.

2.4. Photocatalytic Performance

In practical pollutant removal, organic pollutants usually existed in the mixture of aqueous and organic wastewater. The photodegradation in an aqueous condition has been widely investigated, but that in the organic solution is rarely reported. Herein, we carried out the photodegradation of methyl orange/ethanol solution, examined the photocatalytic activities of various TiO_2/CNF films (**Figure 6**a). After 12h of irradiation, TMP/CNF showed weak activity due to its large particle size and particle agglomeration in the composite film, lowering the

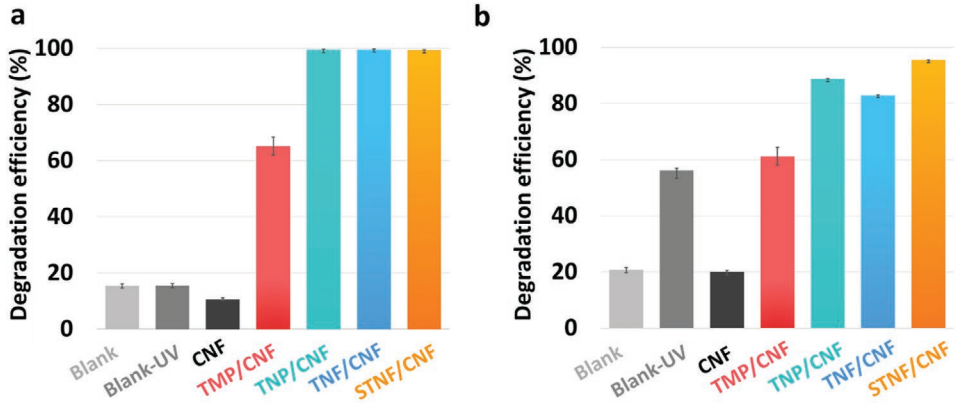

Figure 7. Bar graph plots of degradation efficiency of various TiO_2/CNF composite films toward a) methanol and b) DMF.

surface area. Both TNP/CNF and TNF/CNF showed superior activities to TMP/CNF. It is attributed to the intrinsic highly photocatalytic activities. Also, partial photocatalysts located at the composite surface were observed, and that provided the desirable active surface for organic dye degradation. STNF/CNF showed the highest degradation efficiency at 88% due to the high photoresponse to irradiation (Figure 6b). The photoresponse enhancement was induced by the doping effect of silver and self-precipitation of silver nanoparticles, which was observed by HRTEM (Figure S3, Supporting Information). When Ag is doped into TiO_2, it narrowed the bandgap. Partial Ag dopants assembled at the surface of TiO_2, and formed nanoparticles during calcination. [21] It enhanced the utility of irradiation light due to the surface plasmon resonance, being beneficial to photocatalytic performance. After three recyclability test runs, the degradation efficiency was maintained at around 82% (**Figure 7**c,d).

Furthermore, the photodegradation of methanol and DMF vapors were performed. In the photodegradation of methanol vapor, TNP, TNF, and STNF/CNF films showed excellent degradation efficiencies (Figure 7a), being higher than 95%. For the photodegradation of DMF vapor, though the DMF vapor was self-degraded by UV irradiation, TNP, TNF, and STNF composite films showed great activities (Figure 7b) at least 80%. Interestingly, CNF film in the two degradation tests prevented the vapor from self-degradation. The vapor was adsorbed onto CNF film, and CNF would absorb and screen the UV light for vapor, as mentioned in Figure 4a. The excellent degradation efficiencies of TNP/CNF and TNF/CNF film were observed, being consistent with the MO degradation. Among them, STNF/CNF showed superior degradation efficiency for methanol and DMF. Herein, based on an established investigation of STNF, we concluded the mechanism of the STNF/CNF film toward the organic chemical photodegradation. Through the immobilization of STNF to CNF film, the composite film exhibited solvent resistance and a freestanding appearance. When the bare STNF was irradiated by incident UV light, photoinduced electrons in TiO_2 passed through the Schottky barrier, transferred to self-precipitated silver NPs. The rich electrons coupled with localized electrons of Ag NPs further reacted with oxygen, forming superoxide radicals. The remained holes on TiO_2 NFs promoted the hydroxyl radical formation. Both types of radicals resulted in the redox reaction and degradation of organic pollutants. The possible reaction route is described below. It would be the most significant potential candidate in VOC vapor degradation for practical use in the future

$$TiO_2 + h\nu \rightarrow e^-_{TiO2} + h^+_{TiO2} \quad (2)$$

$$h^+_{TiO2} + H_2O \rightarrow H^+ + \cdot OH \quad (3)$$

$$\cdot OH + \cdot OH \rightarrow O_2 + 2H^+ \quad (4)$$

$$e^-_{TiO2} \rightarrow e^-_{Ag} \quad (5)$$

$$e^-_{Ag} + O_2 \rightarrow \cdot O_2^- \quad (6)$$

$$\cdot O_2^- \text{ and/or } \cdot OH + \text{organic dye} \rightarrow \text{harmless products} \quad (7)$$

2.5. Freestanding CNF Composite Film

In order to demonstrate practicality, we demonstrated the diversity of CNF derived films. Pristine CNF transparent film prepared by the drop-casting method showed high transparency. We can print colorful patterns perfectly on the CNF transparent film using a color laser printer, illustrating its excellent printability (**Figure 8**a). The presence of the same chemical structure of cellulose provided consistent adhesion properties toward the toner that is comparable to pulp-derived paper. This film still maintained a great endurance against several time-bending tests due to the intrinsic mechanical properties attributed to strong inter- and intramolecular hydrogen bonding (Figure 8b). By scaling up the fabrication of such transparent film, it is easy to obtain an A4 size transparent film, as shown in Figure S8 (Supporting Information). Following the same preparation of large-sized transparent film, we can obtain an STNF/CNF film. Its flexibility allows for such film to be folded like a lampshade (Figure 8c).

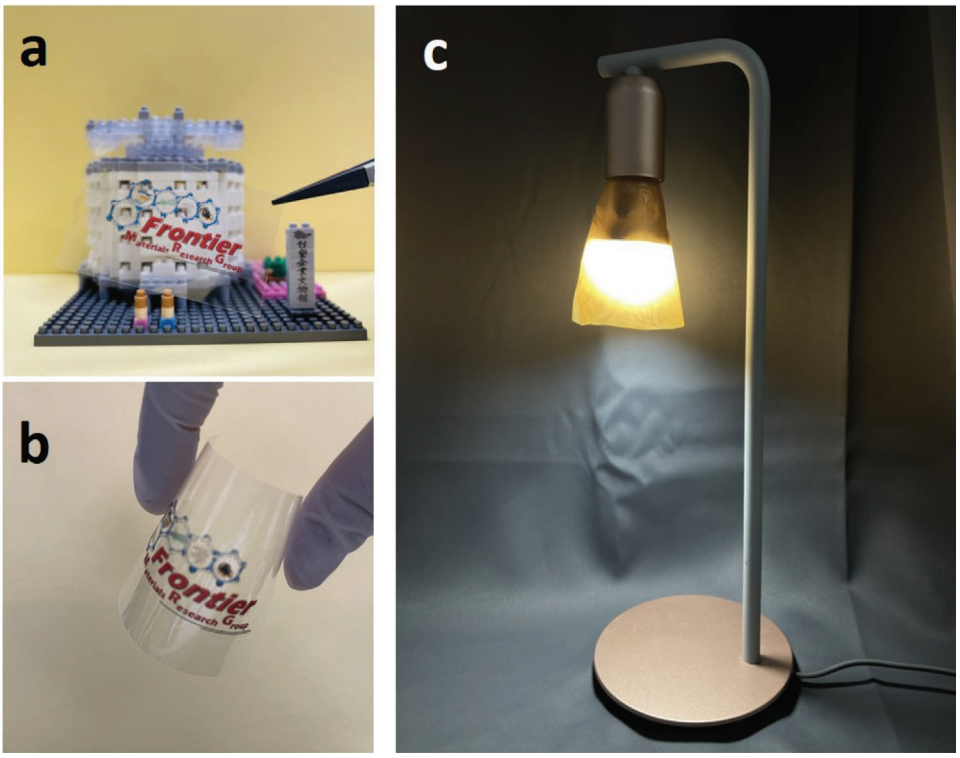

Figure 8. Demonstration of CNF transparent film: a) Color laser printed pristine CNF transparent film, b) the bending test of CNF transparent paper, and c) illustration of the STNF/CNF composite lampshade.

3. Conclusion

Various morphologies of TiO_2, including TMP, TNP, TNF, and STNF, were incorporated with cellulose nanofibers to investigate the morphological matching effect on the CNF composite film. STNF was mainly stacked on the bottom of the composite film and rarely appeared between the oriented CNF without destroying the crystallinity of the CNF film. Various TiO_2/CNF composite films showed outstanding resistance in the acetone and dimethylformamide. Due to its high photoresponse to irradiation, STNF/CNF demonstrated excellent photodegradation capability against methyl orange and VOC vapors, including methanol and DMF. After three runs of the recyclability test, the degradation efficiency for methyl orange was maintained at around 82%. The degradation efficiencies toward methanol and DMF vapor are higher than 90%. Our study demonstrates that STNF/CNF composite films have tremendous practical potentials in eliminating pollutants.

4. Experimental Section

Synthesis of Cellulose Nanofibers and TiO_2 Composite: CNF was synthesized by the TEMPO-mediated oxidation method. Pulp (Chung Hwa Pulp Corporation, laubholz bleached kraft pulp, LBKP), used as raw material, was soaked in the diluted HCl and heated to 100 °C for two h. After several times washed to neutral, 1.0 g of pulp was mixed with 0.025 g of 2,2,6,6-Tetramethylpiperidine-1-oxyl (TEMPO, Acros, 98%) and 0.250 g of sodium bromide (NaBr, Acros, 99.5%) in 200 mL of deionized water. Subsequently, 0.08 mol of sodium hypochlorite (NaClO, Choneye, 12%) was gradually added into the mixture solution, and the pH level was maintained at around 10.0 by adding 0.5 M NaOH and/or $NaHCO_3$ for 24 h. Few sodium thiosulfate pentahydrates ($Na_2S_2O_3{\cdot}5H_2O$, Acros, 99.5%) were added to terminate the oxidation. The postreduction was conducted to decrease the undesirable functional group such as C6 aldehydes and C2/C3 ketones by mixed with sodium borohydride ($NaBH_4$, Acros, 98+%). Lastly, CNF hydrogel was washed several times and collected by centrifugation. To obtain the uniform and superfine CNF, the diluted CNF solution was disintegrated by ultrasonication for 30 min. For the preparation of the composite film, various TiO_2 were preactivated with deionized water under UV irradiation for improving the hydrophilicity. Subsequently, these TiO_2 materials were mixed with diluted CNF hydrogel in the weight ratio of 1:10. After solution casting onto the plastic dish and further dried, a series of TiO_2/CNF circular films with a diameter of ≈7.0 cm were obtained. Here, the TiO_2/CNF composite films consisted of anatase TiO_2 microsized particles (Acros, 99.5+%), AEROXIDETiO_2-P25 nanoparticles (Acros, 100.5%), pristine TiO_2 nanofibers, and Ag-TiO_2 nanofibers were classified by following various sizes and morphologies and noted as TMP, TNP, TNF, and STNF, respectively. Both TNF and STNF were prepared by the hydrothermal method, according to the previous study.[21]

Material Characterization: The morphology of individual CNF and CNF film were observed by atomic force microscopy (Digital Instrument, Nanoscopes III). The crystal structure of composite films was determined by an X-ray diffractometer (Bruker, D2 phaser with Xflash 430, Germany) with Cu Kα radiation at 50.0 kV and 300.0 mA. UV–vis absorption spectra of various TiO_2/CNF composite films were measured by UV–vis spectrophotometer (Jasco, V-730, Japan) in the 400–900 nm of the wavelength range. Cross-sectional image and element mapping were analyzed by multi-function field emission scanning electron microscopy (Hitachi, SU8010, Japan) with energy dispersive spectroscopy (Bruker, XFlash6, Germany). Contact angle measurement was conducted by

using the contact angle meter (Sindatek Instruments, 100SB, Taiwan). Mechanical properties of various TiO_2/CNF composite films were tested by a micro tensile testing machine (Yang Yi Technology Co., Ltd, YH-H31B7, Taiwan), and the regulation of ASTM D638-10 followed the size of the testing samples. Thermogravimetric analysis was conducted by the thermogravimetric analyzer (TA Instruments, TGA Q50, USA). Grazing-incidence wide-angle X-ray scattering (GIWAXS) patterns were acquired by synchrotron X-ray spectroscopy at beamline 13A1 of the National Synchrotron Radiation Research Center (NSRRC), Hsinchu, Taiwan.

Photocatalytic Experiment: For the photodegradation of organic dye, methyl orange (MO, Acros, pure) was chosen as the target. A piece of the composite film was soaked in the 250.0 mL mixture solution of 1.0 ppm methyl orange and ethanol and irradiated under the UV-B illumination (Sankyo Denki, G8T5E, $\lambda_{max} \approx 312$ nm, 8.0 W). Two pieces of the lamp were placed above the reactor with a distance of 10.0 cm. At various time interval, the MO suspension was sampled, and the MO concentration was examined by UV–vis spectrophotometer (JASCO, V-730, Japan). In the photodegradation of VOC vapor, methanol and dimethylformamide (DMF) were used as the targets. The VOC liquid was dropped into a quartz-made reactor with a volume of 500.0 mL and then evaporated. Next, the composite film was put in the reactor and irradiated under two pieces of UV-B lamp. Also, the VOC vapor was sampled at various time intervals by using a 1.0 mL gas-tight syringe. The concentration of VOC vapor was measured by gas chromatographer (Thermo, TraceGC ultra, USA).

Supporting Information

Supporting Information is available from the Wiley Online Library or from the author.

Acknowledgements

T.-H.L., Y.-H.L., and K.-M.L. contributed equally to this work. The authors appreciate Dr. Ming-Tao Lee (BL-13A1) and Dr. Jyh-Fu Lee (BL-17C1) at National Synchrotron Radiation Research Centre for useful discussion and suggestions. We also thank Miss Y.-M. Chang at Instrumentation Centre of National Tsing Hua University for spherical-aberration corrected field emission TEM analysis. The financial support from Ministry of Science and Technology, Taiwan (Project No. 110-2221-E-182-044, and 110-2628-E-182-001), Chang Gung University (QZRPD181), Chang Gung Memorial Hospital, Linkou (CMRPD2J0042 and BMRPC74), Formosa Plastics Group is highly appreciated.

Conflict of Interest

The authors declare no conflict of interest.

Data Availability Statement

Research data are not shared.

Keywords

cellulose nanofibers, composite films, photocatalysts, solvent resistance, volatile organic compound degradation

Received: August 11, 2021
Revised: September 12, 2021
Published online: October 23, 2021

[1] A. Ansari, D. Nematollahi, *Appl. Catal., B* **2020**, *261*, 118226.
[2] N. H. Ismail, W. N. W. Salleh, A. F. Ismail, H. Hasbullah, N. Yusof, F. Aziz, J. Jaafar, *Sep. Purif. Technol.* **2020**, *233*, 116007.
[3] M. Kamali, D. P. Suhas, M. E. Costa, I. Capela, T. M. Aminabhavi, *Chem. Eng. J.* **2019**, *368*, 474.
[4] C. Lai, M. M. Zhang, B. S. Li, D. L. Huang, G. M. Zeng, L. Qin, X. G. Liu, H. Yi, M. Cheng, L. Li, Z. Chen, L. Chen, *Chem. Eng. J.* **2019**, *358*, 891.
[5] L. Liu, Y. H. Qi, J. R. Lu, S. L. Lin, W. J. An, Y. H. Liang, W. Q. Cui, *Appl. Catal., B* **2016**, *183*, 133.
[6] W. D. Oh, L. W. Lok, A. Veksha, A. Giannis, T. T. Lim, *Chem. Eng. J.* **2018**, *333*, 739.
[7] C. V. Reddy, I. N. Reddy, K. R. Reddy, S. Jaesool, K. Yoo, *Electrochim. Acta* **2019**, *317*, 416.
[8] T. Tavangar, M. Karimi, M. Rezakazemi, K. R. Reddy, T. M. Aminabhavi, *Chem. Eng. J.* **2020**, *385*, 123787.
[9] Q. Guo, C. Y. Zhou, Z. B. Ma, X. M. Yang, *Adv. Mater.* **2019**, *31*.
[10] R. F. Qian, H. X. Zong, J. Schneider, G. D. Zhou, T. Zhao, Y. L. Li, J. Yang, D. W. Bahnemann, J. H. Pan, *Catal. Today* **2019**, *335*, 78.
[11] F. Lopes, M. D. C. da Rocha, P. Bargiela, H. S. Ferreira, C. A. D. Pires, *Chem. Eng. Sci.* **2020**, *227*, 115939.
[12] M. A. Mohamed, W. N. W. Salleh, J. Jaafar, A. F. Ismail, M. Abd Mutalib, N. A. A. Sani, S. Asri, C. S. Ong, *Chem. Eng. J.* **2016**, *284*, 202.
[13] H. Wu, T. Inaba, Z.-M. Wang, T. Endo, *Appl. Catal. B* **2020**, *276*, 119111.
[14] M. Ge, C. Cao, J. Huang, S. Li, Z. Chen, K.-Q. Zhang, S. S. Al-Deyab, Y. Lai, *J. Mater. Chem. A* **2016**, *4*, 6772.
[15] M. Z. Ge, Q. S. Li, C. Y. Cao, J. Y. Huang, S. H. Li, S. N. Zhang, Z. Chen, K. Q. Zhang, S. S. Al-Deyab, Y. K. Lai, *Adv. Sci.* **2017**, *4*, 1600152.
[16] J. X. Low, B. Cheng, J. G. Yu, *Appl. Surf. Sci.* **2017**, *392*, 658.
[17] H. Safajou, H. Khojasteh, M. Salavati-Niasari, S. Mortazavi-Derazkola, *J. Colloid Interface Sci.* **2017**, *498*, 423.
[18] J. Y. Zhang, G. C. Xiao, F. X. Xiao, B. Liu, *Mater. Chem. Front.* **2017**, *1*, 231.
[19] V. Kurnaravel, S. Mathew, J. Bartlett, S. C. Pillai, *Appl. Catal., B* **2019**, *244*, 1021.
[20] M.-C. Wu, P.-Y. Wu, T.-H. Lin, T.-F. Lin, *Appl. Surf. Sci.* **2018**, *430*, 390.
[21] M.-C. Wu, T.-H. Lin, K.-H. Hsu, J.-F. Hsu, *Appl. Surf. Sci.* **2019**, *484*, 326.
[22] Y. Nakamura, Y. Ono, T. Saito, A. Isogai, *Cellulose* **2019**, *26*, 6529.
[23] D. Trache, M. H. Hussin, M. K. M. Haafiz, V. K. Thakur, *Nanoscale* **2017**, *9*, 1763.
[24] S. J. Eichhorn, A. Dufresne, M. Aranguren, N. E. Marcovich, J. R. Capadona, S. J. Rowan, C. Weder, W. Thielemans, M. Roman, S. Renneckar, W. Gindl, S. Veigel, J. Keckes, H. Yano, K. Abe, M. Nogi, A. N. Nakagaito, A. Mangalam, J. Simonsen, A. S. Benight, A. Bismarck, L. A. Berglund, T. Peijs, *J. Mater. Sci.* **2010**, *45*, 1.
[25] H. Kargarzadeh, M. Mariano, D. Gopakumar, I. Ahmad, S. Thomas, A. Dufresne, J. Huang, N. Lin, *Cellulose* **2018**, *25*, 2151.
[26] T. Li, J. Song, X. Zhao, Z. Yang, G. Pastel, S. Xu, C. Jia, J. Dai, C. Chen, A. Gong, F. Jiang, Y. Yao, T. Fan, B. Yang, L. Wågberg, R. Yang, L. Hu, *Sci. Adv.* **2018**, *4*, eaar3724.
[27] O. Nechyporchuk, M. N. Belgacem, J. Bras, *Ind. Crops Prod.* **2016**, *93*, 2.
[28] M. Zhao, F. Ansari, M. Takeuchi, M. Shimizu, T. Saito, L. A. Berglund, A. Isogai, *Nanoscale Horiz.* **2018**, *3*, 28.
[29] R. Kubo, T. Saito, A. Isogai, *Cellulose* **2019**, *26*, 4313.
[30] T. Kurihara, A. Isogai, *Cellulose* **2015**, *22*, 2607.
[31] B. Puangsin, H. Soeta, T. Saito, A. Isogai, *Cellulose* **2017**, *24*, 3767.
[32] Z. Q. Shi, H. Y. Xu, Q. L. Yang, C. X. Xiong, M. C. Zhao, K. Kobayashi, T. Saito, A. Isogai, *Carbohydr. Polym.* **2019**, *225*, 115215.
[33] Q. L. Yang, Z. Q. Shi, Z. D. Qi, J. W. Yang, J. Lao, T. Saito, C. Xiong, A. Isogai, *J. Controlled Release* **2017**, *259*, e115.

[34] A. Isogai, T. Hanninen, S. Fujisawa, T. Saito, *Prog. Polym. Sci.* **2018**, *86*, 122.
[35] A. Isogai, T. Saito, H. Fukuzumi, *Nanoscale* **2011**, *3*, 71.
[36] A. Snyder, Z. Bo, R. Moon, J.-C. Rochet, L. Stanciu, *J. Colloid Interface Sci.* **2013**, *399*, 92.
[37] J. X. Wang, W. X. Liu, H. D. Li, H. L. Wang, Z. Wang, W. J. Zhou, H. Liu, *Chem. Eng. J.* **2013**, *228*, 272.
[38] M. C. Wu, A. Sapi, A. Avila, M. Szabo, J. Hiltunen, M. Huuhtanen, G. Toth, A. Kukovecz, Z. Konya, R. Keiski, W. F. Su, H. Jantunen, K. Kordas, *Nano Res.* **2011**, *4*, 360.
[39] S. Banerjee, D. D. Dionysiou, S. C. Pillai, *Appl. Catal. B* **2015**, *176–177*, 396.
[40] T.-H. Lin, M.-C. Wu, K.-P. Chiang, Y.-H. Chang, J.-F. Hsu, K.-H. Hsu, K.-M. Lee, *J. Taiwan Inst. Chem. Eng.* **2021**, *120*, 291.